JACS
JOURNAL OF THE AMERICAN CHEMICAL SOCIETY

Article

pubs.acs.org/JACS

Solid-State Redox Switching of Magnetic Exchange and Electronic Conductivity in a Benzoquinoid-Bridged Mn^{II} Chain Compound

Ie-Rang Jeon,[†] Lei Sun,[‡] Bogdan Negru,[†] Richard P. Van Duyne,[†] Mircea Dincă,[‡] and T. David Harris*[,†]

[†]Department of Chemistry, Northwestern University, 2145 Sheridan Road, Evanston, Illinois 60208-3113, United States
[‡]Department of Chemistry, Massachusetts Institute of Technology, Cambridge, Massachusetts 02139-4307, United States

Supporting Information

ABSTRACT: We demonstrate that incorporation of a redox-active benzoquinoid ligand into a one-dimensional chain compound can give rise to a material that exhibits simultaneous solid-state redox switching of optical, magnetic, and electronic properties. Metalation of the ligand 4,5-bis(pyridine-2-carboxamido)-1,2-catechol ($^{N,O}LH_4$) with Mn^{III} affords the chain compound $Mn(^{N,O}L)(DMSO)$. Structural and spectroscopic analysis of this compound show the presence of Mn^{II} centers bridged by $^{N,O}L^{2-}$ ligands, resulting partially from a spontaneous ligand-to-metal electron transfer. Upon soaking in a solution of the reductant Cp_2Co, $Mn(^{N,O}L)(DMSO)$ undergoes a ligand-centered solid-state reduction to $[Mn(^{N,O}L)]^-$, as revealed by a suite of techniques, including Raman and X-ray absorption spectroscopy. The ligand-based reduction engenders a dramatic modulation of the physical properties of the chain compound. An electrochromic response, evidenced by a color change from dark green to dark purple is accompanied by a nearly 40-fold increase in magnetic coupling strength, from $J = -0.38(1)$ to $-15.6(2)$ cm^{-1}, and a 10,000-fold increase in electronic conductivity, from $\sigma = 2.33(1) \times 10^{-12}$ S/cm ($E_a = 0.64(1)$ eV) to $8.61(1) \times 10^{-8}$ S/cm ($E_a = 0.39(1)$ eV). Importantly, the chemical reduction is reversible: treatment of the reduced compound with $[Cp_2Fe]^+$ regenerates the oxidized chain. Taken together, these results highlight the ability of benzoquinoid ligands to facilitate solid-state ligand-based redox reactions in nonporous coordination solids, giving rise to reversible switching of optical properties, magnetic exchange interactions, and electronic conductivity.

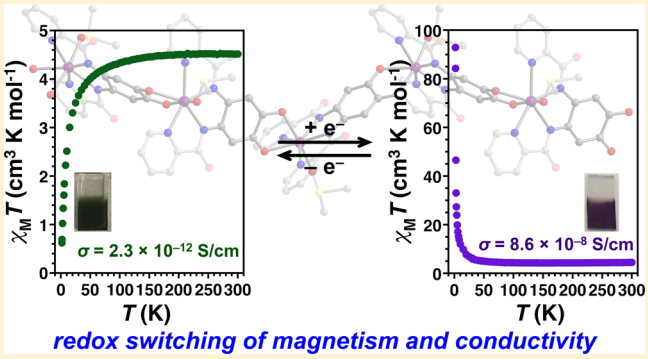

INTRODUCTION

The ability to manipulate the properties of materials is a cornerstone of modern synthetic chemistry. However, the versatility extended to molecular materials or polymers by organic chemistry is not readily translated to inorganic solid-state materials, whose simpler building units do not afford the same opportunities for synthetic control. It is thus the combination of organic ligand manipulation and the complex electronic structure of metal ions that may give rise to a new generation of multifunctional hybrid organic−inorganic materials, which could contribute to the development of advanced electronic devices for information storage and processing, energy storage and conversion, and sensing and switching technology.[1−5] Inorganic solids, such as intermetallic compounds, metal oxides, and metal cyanides, have been successful for the development of inorganic multifunctional materials,[6] owing largely to the presence of long-range electronic and magnetic communication facilitated by optimized orbital overlap, itinerant electrons, and crystalline composition. Nevertheless, despite notable advances, there remains tremendous demand for materials that feature more facile and rapid synthetic accessibility, solution processability, and greater chemical tunability for incorporating and optimizing multiple functionalities.

In targeting multifunctional materials, the employment of organic bridging ligands can afford metal−organic extended solids with programmable and tunable physical functionalities. This strategy has led to a number of solids that feature multiple physical functions, such as unusual magnetic behavior, electronic conductivity, and optical responses. In most of these cases, the various properties can only be addressed independently because they are each controlled by different orthogonal components within a given material.[7−10] Nevertheless, coupling these properties and rendering them interdependent on each other would give rise to novel functions and emergent phenomena that are not associated with the constituent building units.[11] Such materials, which will behave differently than the sum of their parts, may allow for simultaneous switching of multiple coupled properties through a single external stimulus, such as light, magnetic field, or electrical current.

Received: March 7, 2016
Published: April 26, 2016

DOI: 10.1021/jacs.6b02485
J. Am. Chem. Soc. 2016, 138, 6583−6590

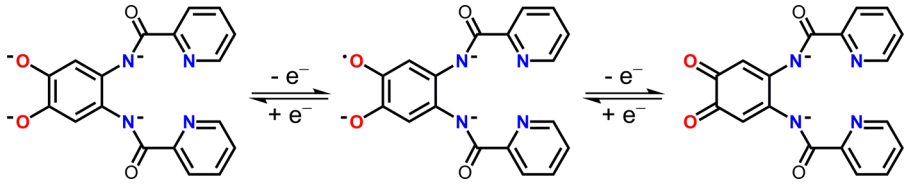

Figure 1. Redox series of deprotonated benzoquinoid ligands involved in this report: left to right, $^{N,O}L^{4-}$, $^{N,O}L^{3-\bullet}$, $^{N,O}L^{2-}$.

Considering potential organic bridging ligands to support simultaneous control of magnetic, electronic, and optical properties in an extended solid, benzoquinoid ligands offer several key attributes. These ligands readily undergo redox chemistry to stabilize both diamagnetic benzoquinoid and paramagnetic semiquinoid redox isomers. Their incorporation into metal complexes has given rise to molecules with controllable optical properties,[12] strong magnetic exchange, and charge delocalization.[13,14] Indeed, an extended solid that contains paramagnetic metal ions connected by semiquinoid ligands should feature long-range electronic communication and strong direct magnetic exchange, as has recently been demonstrated in ferric semiquinoid solids.[15,16] In addition, by virtue of their inherent ligand redox activity, metal semiquinoid compounds offer an ideal platform for the realization of redox-switchable materials.

Here, we demonstrate that the asymmetric benzoquinoid ligand 4,5-bis(pyridine-2-carboxamido)-1,2-catechol ($^{N,O}LH_4$),[17] which can be accessed in three oxidation states (see Figure 1), directs the synthesis of the chiral chain compound Mn(^{N,O}L)(DMSO). This compound can be reduced postsynthetically, in the solid state, by one electron to afford the compound [Cp_2Co][Mn(^{N,O}L)]. The latter compound features a semiquinoid radical-bridged Mn^{II} chain and exhibits a significant enhancement in both magnetic exchange and electronic conductivity compared with the neutral compound. In sum, we report a rare system that allows for reversible switching of optical, magnetic, and electronic properties in the solid state through a one-electron redox event that serves as a single external stimulus.

EXPERIMENTAL SECTION

General Considerations. The manipulations described herein were performed under a dinitrogen atmosphere in an MBraun LABstar glovebox operated under a humid, oxygen-free atmosphere, or in a Vacuum Atmospheres Nexus II water- and oxygen-free glovebox. *N*,*N*-Dimethylformamide (DMF), tetrahydrofuran (THF), and acetonitrile (MeCN) were dried using a commercial solvent purification system from Pure Process Technology. THF and MeCN were stored over 3 Å molecular sieves prior to use. Effective removal of oxygen and moisture in THF was verified using a standard purple solution of sodium benzophenone ketyl. 4,5-Bis(pyridine-2-carboxamido)-1,2-catechol ($^{N,O}LH_4$) was prepared according to a reported literature procedure.[17] All other reagents were purchased from commercial vendors and used without further purification.

Mn(^{N,O}L)(DMSO) (1). To a DMF solution (4 mL) of $^{N,O}LH_4$ (0.550 g, 1.57 mmol) was added dropwise with stirring a brown mixture of $Mn(CH_3COO)_3{\cdot}2H_2O$ (0.850 g, 3.17 mmol) in DMF (12 mL) to give a dark green solution. After stirring at ambient temperature for 12 h, the resulting dark mixture was filtered through a nylon membrane (0.22 μm) to give a dark green solid residue. The residue was dissolved in DMSO (60 mL) in air, and subsequent diffusion of diethyl ether vapor into the resulting solution yielded **1** (0.650 g, 80%) as dark green needle-shaped crystals suitable for X-ray analysis. Anal. Calcd for $C_{20}H_{20}MnN_4O_7S$ (**1**·$2H_2O$): C, 46.6; H, 3.91; N, 10.8%. Found: C, 46.3; H, 3.29; N, 10.4%. FT-IR (ATR, cm^{-1}): 1632(s); 1562(s); 1469(s); 1167(s); 1079(s); 953(w); 935(m); 702(m); 674(m).

[Cp_2Co][Mn(^{N,O}L)] (1^{red}). Dark green crystalline **1** (0.100 g, 0.194 mmol) was added to a solution of Cp_2Co (0.100 g, 0.529 mmol) in a 1:1 THF/MeCN mixture (20 mL). After 24 h, the supernatant was decanted and replaced with a fresh solution of Cp_2Co (0.100 g, 0.529 mmol) in a 1:1 THF/MeCN mixture (20 mL). After an additional 24 h, the supernatant was again decanted, and the solid was washed with MeCN (3 × 10 mL) and then THF (3 × 10 mL). The solid was then dried for 24 h at 60 °C under reduced pressure to yield $\mathbf{1}^{red}$ (0.105 g, 76%) as a dark purple microcrystalline solid. Anal. Calcd for $C_{28}H_{20}MnCoN_4O_4$ ($\mathbf{1}^{red}$): C, 57.0; H, 3.42; N, 9.49%. Found: C, 56.5; H, 3.70; N, 9.60%. ICP-AES analysis found a Co/Mn mass ratio of 0.52:0.48, within the standard 5% instrumental error of 1:1. FT-IR (ATR, cm^{-1}): 3080 (w); 1576 (s); 1523(s); 1469(s); 1410(m); 1344(s); 1009(m); 930(m); 758(m); 702(m); 460(s).

Mn(^{N,O}L) (1^{ox}). Dark purple crystalline $\mathbf{1}^{red}$ (50.0 mg, 0.0707 mmol) was added to a solution of [Cp_2Fe](BF_4) (37.5 mg, 0.113 mmol) in a 1:1 THF/MeCN mixture (10 mL). After 24 h, the supernatant was decanted and replaced with a fresh solution of [Cp_2Fe](BF_4) (37.5 mg, 0.113 mmol) in a 1:1 THF/MeCN mixture (10 mL). After an additional 24 h, the supernatant was again decanted, and the solid was washed with MeCN (3 × 5 mL) and then THF (3 × 5 mL). The solid was then dried for 24 h at 60 °C under reduced pressure to yield $\mathbf{1}^{ox}$ (27.0 mg, 87%) as a dark green microcrystalline solid. Anal. Calcd for $C_{18}H_{14}MnN_4O_6$ ($\mathbf{1}^{ox}{\cdot}2H_2O$): C, 49.4; H, 3.23; N, 12.8%. Found: C, 49.1; H, 2.93; N, 12.3%. FT-IR (ATR, cm^{-1}): 1632(s); 1562(s); 1469(s); 1167(s); 1079(s); 935(m); 702(m); 674(m).

X-ray Structure Determination. A single crystal of **1** suitable for X-ray analysis was coated with Paratone-N oil and mounted on a MicroMounts rod. The crystallographic data were collected at 100 K on a Bruker APEX II diffractometer equipped with Cu Kα microsource. Raw data were integrated and corrected for Lorentz and polarization effects using Bruker APEX2 v. 2009.1,[18] and absorption corrections were applied using SADABS.[19] The space group assignment was determined by examination of systematic absences, E-statistics, and successive refinement of the structures. The structure was solved and refined with SHELXL[20] operated with the OLEX interface.[21] Hydrogen atoms were placed at calculated positions using suitable riding models and refined using isotropic displacement parameters derived from their parent atoms. Thermal parameters were refined anisotropically for all non-hydrogen atoms. Crystallographic data and the details of data collection are given in Table 1.

Powder X-ray Diffraction. Compounds **1**, $\mathbf{1}^{red}$, and $\mathbf{1}^{ox}$ were each transferred to a boron-rich capillary tube with a 0.7 mm outer diameter. The tube containing $\mathbf{1}^{red}$ was capped with a septum in a nitrogen-filled glovebox, evacuated on a Schlenk line outside of the glovebox while in liquid nitrogen, and flame-sealed. Powder X-ray diffraction patterns were collected on a Rigaku ATXG diffractometer equipped with Cu Kα radiation. The tube voltage and current were 50 kV and 240 mA, respectively.

X-ray Absorption Spectroscopy. X-ray absorption near edge structure spectroscopy (XANES) data were collected at the Advanced Photon Source of Argonne National Laboratory on Beamline 5-BM-D. The radiation was monochromated by a Si(111) double-crystal monochromator. All samples were measured in transmission mode, with powder samples contained within a boron-rich capillary tube. The energy was calibrated with a Mn foil for the Mn edge at 6539 eV. All data were collected at ambient temperature. Data reduction of the spectra was performed using the ATHENA program.[22]

DOI: 10.1021/jacs.6b02485
J. Am. Chem. Soc. 2016, 138, 6583−6590

Table 1. Crystallographic Data for 1

empirical formula	$C_{20}H_{16}MnN_4O_5S$
formula wt, g mol^{-1}	479.37
cryst. syst.	trigonal
space group	$P3_1$
wavelength, Å	1.54178
temp, K	100
a, Å	9.1358(2)
b, Å	9.1358(2)
c, Å	21.2002(6)
α, deg	90
β, deg	90
γ, deg	120
V, Å^3	1532.37(8)
Z	3
ρ_{calcd}, mg m^{-3}	1.558
μ, mm^{-1}	6.576
reflns coll./unique	12254/3130
R(int)	0.0295
R_1[a] ($I > 2\sigma(I)$)	0.0242
wR_2[b] (all)	0.0615
GOF	1.029

[a] $R_1 = \sum||F_o| - |F_c||/\sum|F_o|$. [b] $wR_2 = [\sum w(F_o^2 - F_c^2)^2/\sum w(F_o^2)^2]^{1/2}$.

Electrophoretic Deposition. Crystalline samples of **1** and **1**^{red} (10 mg each) were ground and dispersed in toluene (20 mL) and sonicated for 5 min to give a dark green and dark purple suspension, respectively. Two identical fluorine-doped tin oxide (FTO) glass substrates (15 Ω/sq, Hartford Glass) were dipped into this mixture with a separation distance of 1 cm, and a constant dc voltage of 140 V was applied using an Agilent E3 612 dc power supply for 30 min.

Magnetic Measurements. Magnetic data of **1**, **1**^{red}, and **1**^{ox} were collected on polycrystalline samples, each sealed in a polyethylene bag. The sample for **1**^{red} was manipulated and sealed under a dinitrogen atmosphere. All data were collected using a Quantum Design MPMS-XL SQUID magnetometer from 1.8 to 300 K at applied dc fields ranging from 0 to +7 T. The dc susceptibility data were corrected for diamagnetic contributions from the sample holder and for the core diamagnetism of each sample, estimated using Pascal's constants.[23]

Raman Spectroscopy. Raman spectra were collected using a Nikon Eclipse Ti−U inverted microscope for crystalline samples of **1** and **1**^{ox} on a cover glass and for **1**^{red} and **2**, which were transferred to a quartz Schlenk cuvette under a dinitrogen atmosphere. Renishaw HPNIR 785 nm, Voltex 633 nm, Spectra Physics Excelsior 532 nm, and Micro Laser Systems 405 nm continuous-wave diode lasers were each focused with a 20× objective (NA = 0.45) onto individual crystals. The scattered light was then collected and focused onto the entrance slit of an Acton SpectraPro 2500i spectrograph (Princeton Instruments) fitted with a 1200 grooves/mm or a 600 grooves/mm grating (blaze at 750 and 500 nm, respectively) and a back-illuminated Pixis 400BR charge-coupled device (Princeton Instruments). The spectra were typically acquired for 30−100 s with laser powers at 200 to 1000 μW. Background spectra of the sample holder were subtracted from the sample spectra.

Other Physical Measurements. Elemental analyses of **1**, **1**^{red}, and **1**^{ox} were performed by the Midwest Microlab (Indianapolis, IN). Inductively coupled plasma atomic emission spectra were collected on a Thermo iCAP 7600 ICP-OES instrument. Infrared spectra were recorded on a Bruker Alpha FTIR spectrometer equipped with an attenuated total reflectance accessory. Absorption spectra were taken with a CARY 5000 UV−vis−NIR spectrophotometer. Cyclic voltammetry measurements were carried out in a standard one-compartment cell under dinitrogen, equipped with a **1**-deposited FTO film as a working electrode, a platinum wire as a counter electrode, and a 0.01 M Ag/AgNO$_3$ as a reference electrode using a CHI 660E

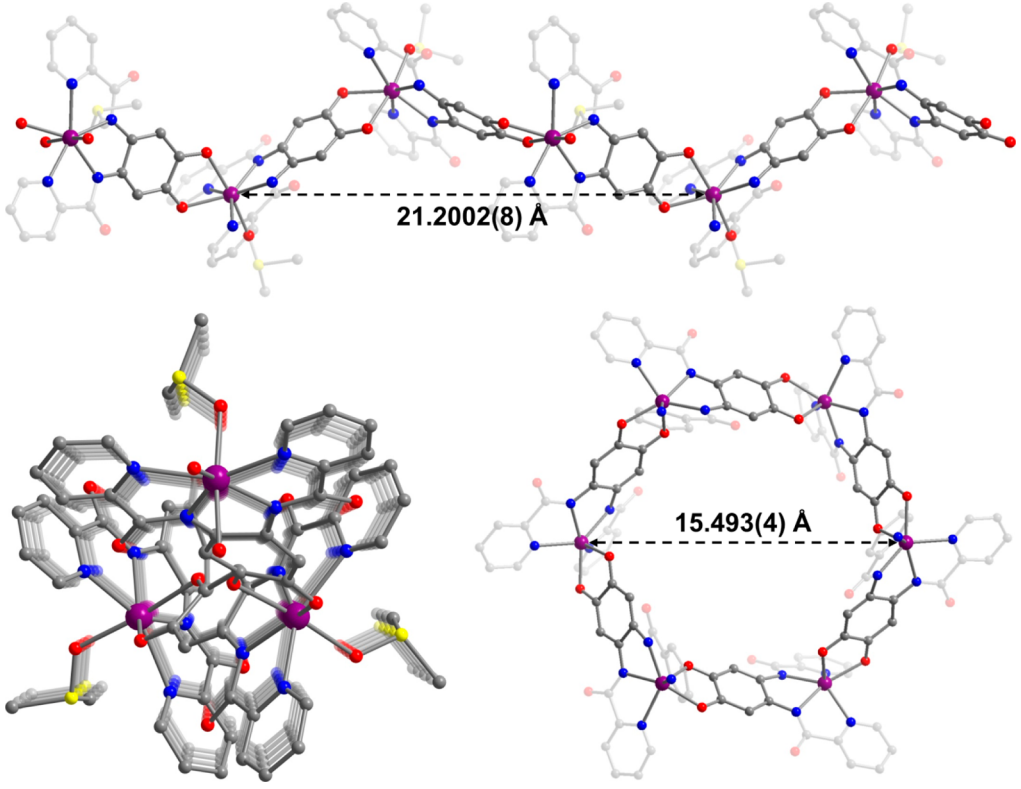

Figure 2. X-ray crystal structures of **1**, as viewed along the crystallographic a (upper) and c (lower left) axes, and $[Mn^{II}_6(^{N,O}L^{3-\bullet})_6]^{6-}$ (lower right), as observed in **2** (ref 17). Purple, yellow, red, blue, and gray spheres represent Mn, S, O, N, and C atoms, respectively; H atoms are omitted and portions of $^{N,O}L^{n-}$ and DMSO are faded for clarity.

DOI: 10.1021/jacs.6b02485
J. Am. Chem. Soc. 2016, 138, 6583−6590

potentiostat. Analyte solutions were prepared with 0.05 M solutions of $(Bu_4N)PF_6$ in MeCN. XPS data were collected on a Kratos AXIS Nova (X-ray diffraction and photoelectron spectroscopy facilities at University of Chicago) or on a Thermo Scientific ESCALAB 250Xi (NUANCE at Northwestern University). Two-point dc conductivity data were collected in a dinitrogen-filled glovebox at 300 K using a home-built press and a Keithley 6517B electrometer, as previously described.[24] The powder was pressed between two steel rods of 2 mm diameter inside of a glass capillary. The thickness of the pressed pellets typically ranged from 0.1 to 0.5 mm. Variable-temperature dc conductivity data were collected with a home-built two-screw press[16] and a Keithley 6517B electrometer (or a Keithley 2450 sourcemeter) between 300 and 390 K. The powder was pressed between two stainless steel screws inside of a plastic tube made of Garolite 10. The pressed pellets were prepared in a dinitrogen-filled glovebox, transferred into a Janis probe station (ST-500) through a miniature vacuum transfer chamber, and kept under dark environment and in vacuum ($\sim 10^{-5}$ Torr).

RESULTS AND DISCUSSION

Synthesis, Structures, and Electrochemistry. Reaction of $Mn(CH_3COO)_3{\cdot}2H_2O$ with $^{N,O}LH_4$ in DMF at 25 °C resulted in a dark green precipitate. Dissolution of this precipitate in DMSO, followed by diffusion of diethyl ether vapor into the resulting solution, yielded dark green needle-shaped crystals of $Mn(^{N,O}L)(DMSO)$ (**1**) in 80% yield. Single-crystal X-ray analysis revealed that **1** crystallizes in the chiral, trigonal space group $P3_1$, with a global structure comprised of 3-fold helical chains that contain Mn centers connected by deprotonated $^{N,O}L^{n-}$ ligands (see Figure 2, upper). Each chain is situated along the crystallographic *c* axis, with a helix pitch of 21.2002(8) Å that corresponds to the length of the unit cell. Along the chain, each Mn center is crystallographically related to the next through a 3-fold screw axis. The structure of **1** features shortest intra- and interchain Mn···Mn distances of 8.422(1) Å and 8.932(1) Å, respectively, with the latter value highlighting a close-packed arrangement between adjacent chains without significant porosity of the solid.

Each Mn center resides in a distorted pentagonal bipyramidal coordination environment, where the equatorial N_4 plane is formed by nitrogen donor atoms from two pyridyl and two carboxamido groups of $^{N,O}L^{n-}$, while two adjacent sites are occupied by oxygen donor atoms from the *o*-catechol moiety of a second molecule of $^{N,O}L^{n-}$. The additional axial position is occupied by the oxygen atom of a DMSO molecule. The mean respective Mn−N and Mn−O distances of 2.297(3) and 2.291(2) Å, in conjunction with the heptacoordinate Mn ion, unambiguously confirm a high-spin Mn^{II} electronic configuration. The overall neutral charge of the chain therefore implies the presence of $^{N,O}L^{2-}$ bridging ligands.

To probe and confirm the dianionic electronic configuration $^{N,O}L^{2-}$ of the bridging ligand, bond distances involving benzoquinoid atoms were carefully inspected. The mean quinoid C−C distance of 1.439(5) Å is 2.1% longer than that observed for $^{N,O}L^{3-\bullet}$, 1.41(2) Å, in the related molecular compound $[Cp_2Co]_6[Mn_6(^{N,O}L)_6]{\cdot}8DMSO$ (**2**, see Figure 2, lower right),[17] indicative of a lower net C−C bond order in **1**. Concordant with this observation, the mean C−O and C−N distances of 1.250(4) and 1.349(4) Å, respectively, fall 3.2% and 1.6% shorter than those in **2**, 1.29(2) and 1.37(2) Å. Moreover, the distances in **1** are consistent with those previously reported in molecular complexes containing diamagnetic, dianionic $^{N,N}L^{2-}$, and $^{O,O}L^{2-}$ ligands.[13b,c,25] Taken together, these structural observations indicate an electronic composition for **1** of $Mn^{II}(^{N,O}L^{2-})(DMSO)$. This composition implies that the Mn ion and bridging ligand, respectively, undergo a one-electron reduction and a two-electron oxidation during the reaction to form **1**. This redox chemistry likely results from a spontaneous ligand-to-metal electron transfer during the reaction, with excess Mn^{III} providing the additional net one-electron oxidation. Indeed, this scenario is supported by the fact that the isolated yield of **1** is maximized upon using a 2:1 stoichiometric ratio of $Mn(CH_3COO)_3{\cdot}2H_2O$ to $^{N,O}LH_4$ in the reaction.

To investigate the electrochemical behavior of **1**, a thin film was prepared on a fluorine-doped tin oxide (FTO) electrode via electrophoretic deposition.[26] The cyclic voltammogram of this film exhibits a quasi-reversible redox process with anodic and cathodic peaks at −0.30 and −1.35 V vs $Ag^{0/1+}$, respectively (see Figure 3). Based on precedent in benzoquinoid-bridged

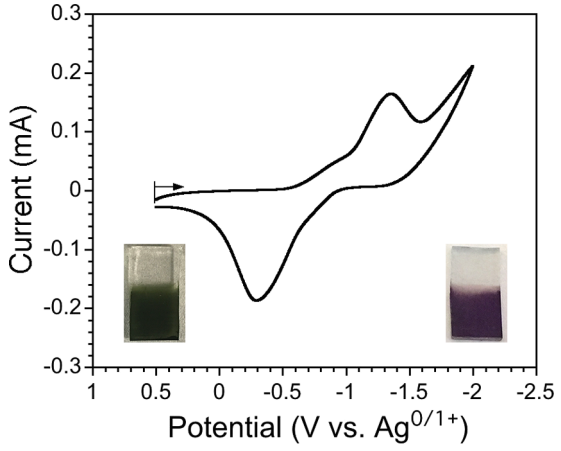

Figure 3. Cyclic voltammogram obtained for a film of **1** deposited on an FTO working electrode, with a 50 mV/s scan rate and 0.05 M $(Bu_4N)PF_6$ supporting electrolyte. Inset: Optical images of macroscopic films of **1** (left) and $\mathbf{1}^{red}$ (right) deposited on FTO.

molecular complexes,[13,14] we tentatively assign this process to a ligand-based $^{N,O}L^{2-/3-\bullet}$ redox couple. Notably, a significant color change of the film from dark green to dark purple was observed upon cathodic scanning, demonstrating that **1** is a rare example of an electrochromic metal−organic solid.[27] The large peak separation of ΔE = 1.05 V observed for this redox couple can likely be attributed to slow diffusion of the bulky $(Bu_4N)^+$ cations into the structure of the solid film, as has been observed in films of similar materials.[28] Although the cyclic voltammetry enabled the characterization of the main redox process in **1**, note that the film deteriorated upon cycling, presumably due to the insertion of cations, which prohibited further detailed studies.

The observed electrochemical behavior of **1** suggests that the anionic chain $[Mn(^{N,O}L)]^-$ should be chemically accessible. Toward this end, a microcrystalline sample of **1** was soaked in a THF/MeCN solution containing excess Cp_2Co for 48 h. During this time, the dark green solid changed to dark purple as **1** was converted to $[Cp_2Co][Mn(^{N,O}L)]$ ($\mathbf{1}^{red}$), which gradually turned back to green upon exposure to air. Remarkably, this solid-state redox process is reversible, as evidenced by a solid sample of $\mathbf{1}^{red}$ being converted to $Mn(^{N,O}L)$ ($\mathbf{1}^{ox}$) upon soaking in a THF/MeCN solution of $[Cp_2Fe](BF_4)$ for 48 h. Here, the absence of an axial DMSO ligand was revealed by FT-IR and XPS (see Figures S1 and S2). Quantitative one-electron redox

DOI: 10.1021/jacs.6b02485
J. Am. Chem. Soc. 2016, 138, 6583−6590

processes were confirmed for both reductive and oxidative reactions by diffuse-reflectance UV−visible spectroscopy and metals analysis (see Experimental Section and Figure S3).

Interestingly, reaction of Cp_2Co with the precursors $Mn(CH_3COO)_3{\cdot}2H_2O$ with $^{N,O}LH_4$ in DMF, followed by crystallization from DMSO solution, gave **2** rather than $\mathbf{1}^{red}$.[17] This observation suggests that the molecular $[Mn_6(^{N,O}L^{3-\bullet})_6]^{6-}$ complex is more thermodynamically favorable in this solution-based reaction than is a $[Mn(^{N,O}L^{3-\bullet})]^-$ chain, and $\mathbf{1}^{red}$ may therefore represent a metastable product that can only be accessed through solid-state reduction of **1**. Possibly, upon binding two trianionic $^{N,O}L^{3-\bullet}$ ligands, the Mn ion is restricted to a coordination number of 6 such that it cannot accommodate a DMSO molecule into its coordination sphere and thus prompts the formation of a wheel rather than a chain. Indeed, similar effects of solvent coordination have been reported in Cu Schiff-base compounds to determine whether a molecular Cu_3 complex or a helical chain compound forms from solution.[29]

Single crystals of **1** gradually lose their integrity upon soaking in the solution of Cp_2Co, thereby precluding single-crystal X-ray diffraction analysis of $\mathbf{1}^{red}$. Nevertheless, powder X-ray diffraction data collected for a microcrystalline sample of $\mathbf{1}^{red}$ shows a dramatically different diffraction pattern than that of **1** (see Figure 4). Indeed, the absence of any residual diffraction

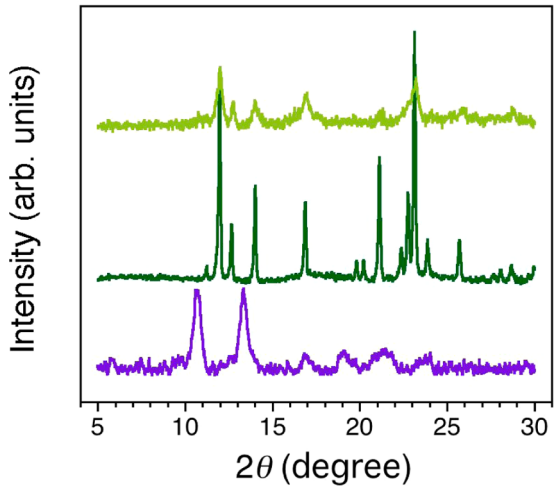

Figure 4. Powder X-ray diffraction patterns for **1** (dark green), $\mathbf{1}^{red}$ (purple), and $\mathbf{1}^{ox}$ (light green).

peaks from **1** indicated a complete reaction, corroborating the optical spectra and metals analysis noted above. The relative loss of crystallinity upon reduction of **1** to $\mathbf{1}^{red}$ likely stems from incorporation of $[Cp_2Co]^+$ cations into the nonporous solid-state structure. Furthermore, the powder X-ray diffraction pattern of $\mathbf{1}^{ox}$ is globally consistent with that of **1**, albeit with considerable further loss of crystallinity, suggesting that the one-dimensional network is preserved during the redox reactions.

Raman and X-ray Absorption Spectroscopy. To further examine the electronic structure of the bridging ligand during solid-state redox reactions, Raman spectra were collected for solid samples of **1**, $\mathbf{1}^{red}$, $\mathbf{1}^{ox}$, and **2** at ambient temperature (see Figures 5 and S4). An initial qualitative comparison of the spectra reveals major similarities between those for **1** and $\mathbf{1}^{ox}$ and those for $\mathbf{1}^{red}$ and **2**. Upon further inspection, the υ_{CC} vibration of the quinoid ring observed at 1390 cm^{-1} for **1** and

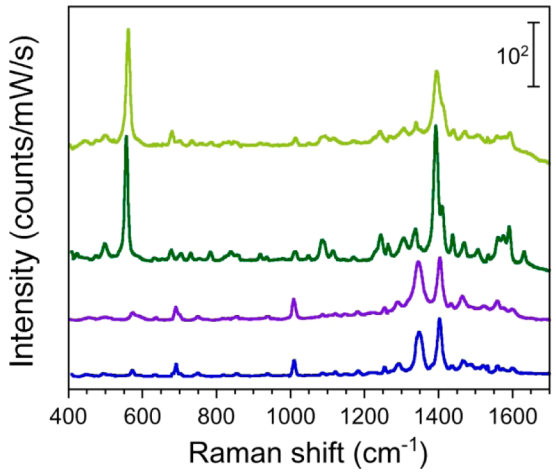

Figure 5. Raman spectra collected for solid samples of **1** (dark green), $\mathbf{1}^{red}$ (purple), $\mathbf{1}^{ox}$ (light green), and **2** (blue) for 100 s with λ_{ext} = 785 nm at 1 mW.

$\mathbf{1}^{ox}$ is shifted lower in energy to 1350 cm^{-1} for $\mathbf{1}^{red}$ and **2**, indicative of higher net C−C bond order. In conjunction with this shift, the intense Raman band at 558 cm^{-1} for **1** and $\mathbf{1}^{ox}$, which can be assigned to an υ_{MO} vibration,[15,30] undergoes a dramatic decrease in intensity and is shifted higher in energy to 573 cm^{-1} for $\mathbf{1}^{red}$ and **2**. In addition, a new band at 1459 cm^{-1} appeared upon reduction, which we assign to the υ_{CO} vibration of the semiquinoid radical.[31] The significant decrease in intensity of the υ_{MO} mode upon reduction likely stems from differences in the resonance enhancement of the mode at 785 nm for the different redox isomers (see Figure S4). Finally, IR spectra collected for solid samples of **1**, $\mathbf{1}^{red}$, and $\mathbf{1}^{ox}$ are consistent with the observed Raman spectral trends (see Figure S1). Taken together, these spectra confirm the presence of ligand-based redox processes upon redox switching between $Mn^{II}(^{N,O}L^{2-})$ and $[Mn^{II}(^{N,O}L^{3-\bullet})]^-$. Note that $\mathbf{1}^{red}$ provides a rare example of a one-dimensional chain comprising paramagnetic metal ions bridged by semiquinoid radical ligands.[32]

In order to confirm the absence of Mn-based redox chemistry, Mn K-edge X-ray absorption spectra were collected for solid samples of **1**, $\mathbf{1}^{red}$, $\mathbf{1}^{ox}$, and **2** (see Figure S5). The spectra for all samples exhibited both pre-edge and main edge features at the identical energies of 6537 and 6545 eV, respectively. Considering that edge energy changes of ca. 3 eV are typically observed upon moving from Mn^{II} to Mn^{III},[33] the invariance of energies across the four compounds provides further strong evidence that the redox chemistry associated with these compounds is indeed ligand-centered.

Electronic Conductivity. To probe and compare the electronic communication in the chain compounds, electronic conductivity measurements were carried out on pressed pellets of **1** and $\mathbf{1}^{red}$ using two-probe dc current−voltage techniques (see Figure S6). For **1**, a conductivity of $\sigma = 2.33(1) \times 10^{-12}$ S/cm was observed at ambient temperature. This value falls in the range of those previously obtained for pressed pellets of Mn^{II} metal−organic solids.[34] In contrast, $\mathbf{1}^{red}$ exhibits a conductivity that is 4 orders of magnitude higher, with an ambient temperature value $\sigma = 8.61(1) \times 10^{-8}$ S/cm. Note that pressed pellet measurements are influenced by interparticle and interchain contact resistance and represent an average value over all crystallographic orientations. In general, single-crystal conductivity values of low-dimensional materials can be 2−3

DOI: 10.1021/jacs.6b02485
J. Am. Chem. Soc. 2016, 138, 6583−6590

orders of magnitude higher.[35] Although a single-crystal measurement of **1** was prohibited due to the small crystallite size and its fragility upon drying, the enhancement upon reduction is likely to be similar in magnitude for single crystals as is observed here for pressed pellets.

Such a dramatic increase in electronic conductivity in a coordination compound upon ligand redox chemistry has been previously observed,[16,36] albeit mostly in compounds that incorporate diamagnetic metal ions or valence-ambiguous metal–ligand compositions. Indeed, **1** and $\mathbf{1}^{red}$ provide a rare example of isolated chain compounds that feature reversible ligand-based redox chemistry. This comparison highlights the importance of charge carrier density on enhancing the electronic conductivity. Moreover, the observed conductive nature of these compounds likely assists the solid-state redox reactions observed within the nonporous crystal structure.

To gain further insight into the observed electronic conductivity, variable-temperature conductivity measurements were performed on pressed pellets of **1** and $\mathbf{1}^{red}$ in the temperature range 300–390 K (see Figure 6). Upon increasing

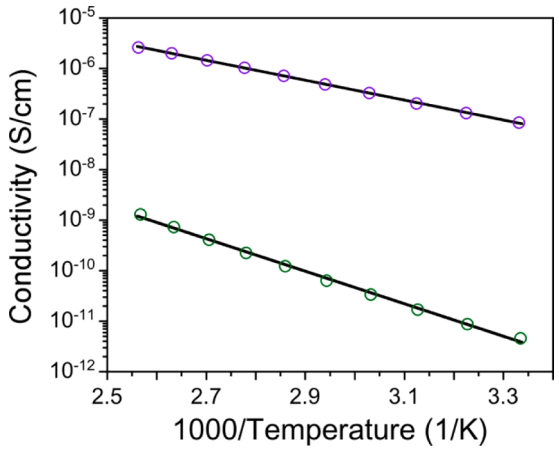

Figure 6. Variable-temperature electronic conductivity data for **1** (green) and $\mathbf{1}^{red}$ (purple), collected on pressed pellets using two-probe current–voltage techniques. The black lines correspond to Arrhenius fits of the data.

temperature, the electronic conductivity of both **1** and $\mathbf{1}^{red}$ increased, showing a linear relationship between the logarithm of conductivity and inverse temperature. This variable-temperature trend indicates that both compounds behave as thermally activated semiconductors. Arrhenius fits to data provide activation energies of E_a = 0.64(1) and 0.39(1) eV for **1** and $\mathbf{1}^{red}$, respectively. The smaller activation energy of $\mathbf{1}^{red}$ can likely be attributed to a shifting of the Fermi level closer to the conduction band as a result of the chemical reduction, similar to the doping of donors in a classic semiconductor.[37] Furthermore, this observation also supports the higher charge density and higher conductivity in $\mathbf{1}^{red}$.

Static Magnetic Properties. To probe potential magnetic interactions in the chain compounds, variable-temperature dc magnetic susceptibility data were collected for solid samples of **1**, $\mathbf{1}^{red}$, and $\mathbf{1}^{ox}$, with the resulting plots of $\chi_M T$ vs T shown in Figure 7. In the case of **1**, the 300 K value of $\chi_M T$ = 4.51 cm^3 K/mol is close to the value of 4.375 cm^3 K/mol expected for magnetically isolated $S = {}^5/_2$ Mn^{II} centers with g = 2. Upon lowering the temperature, $\chi_M T$ remains relatively constant before undergoing a monotonic decrease below 100 K to reach

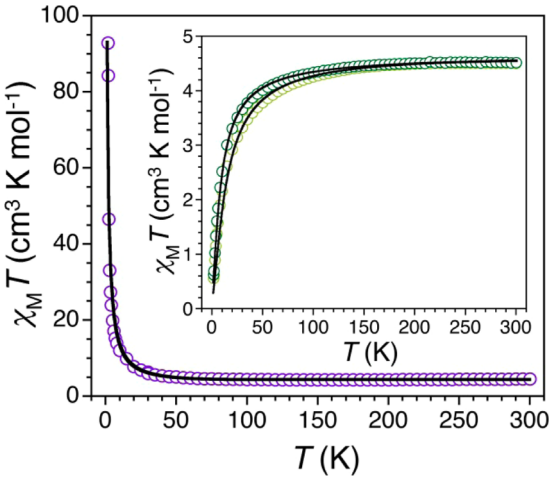

Figure 7. Variable-temperature dc magnetic susceptibility data for $\mathbf{1}^{red}$ (purple), collected under an applied dc field of 0 T. Inset: Variable-temperature dc magnetic susceptibility data for **1** (dark green) and $\mathbf{1}^{ox}$ (light green), collected under an applied dc field of 1 T. The black lines correspond to fits of the data.

a minimum value of 0.6 cm^3 K/mol at 1.8 K. This decrease in $\chi_M T$ with decreasing temperature is indicative of weak antiferromagnetic coupling between Mn^{II} centers. To quantify this interaction, the data were modeled considering a one-dimensional arrangement of classical spins according to the Hamiltonian $\hat{H} = -2J\sum(\hat{S}_{Mn_i} \cdot \hat{S}_{Mn_{i+1}})$.[38] A fit to data gave an exchange constant J = −0.38(1) cm^{-1}, indicative of weak superexchange between Mn^{II} centers though diamagnetic $^{N,O}L^{2-}$ bridges.

In contrast, the plot of $\chi_M T$ vs T obtained for $\mathbf{1}^{red}$ exhibits a dramatically different profile. At 300 K, $\chi_M T$ = 4.53 cm^3 K/mol, slightly lower than the value of 4.75 cm^3 K/mol expected for magnetically noninteracting $S = {}^5/_2$ Mn^{II} centers and $S = {}^1/_2$ ligand radicals, suggesting the presence of antiferromagnetic interactions between the metal ions and the radical ligands. The data undergo a gradual decrease upon lowering temperature, reaching a minimum value of 4.25 cm^3 K/mol at 160 K, followed by an abrupt increase to a maximum of $\chi_M T$ = 92.8 cm^3 K/mol at 1.8 K. This temperature dependence can be attributed to one-dimensional correlation of the S = 2 residual spin units that result from a ferrimagnetic arrangement of $S = {}^5/_2$ Mn^{II} centers and $S = {}^1/_2$ radical ligands. Accordingly, a fit to the data considering a chain model for alternating classical ($S = {}^5/_2$) and quantum ($S = {}^1/_2$) spins, considering the Hamiltonian $\hat{H} = -2J\sum[(\hat{S}_{Mn_i} + \hat{S}_{Mn_{i+1}})\cdot\hat{S}_{L_i}]$,[39] provided an estimated coupling constant of J = −15.6(2) cm^{-1} that corresponds to coupling between Mn^{II} and $^{N,O}L^{3-\bullet}$. This value is in agreement with that of J = −15.6(4) cm^{-1} previously reported for the interaction between Mn^{II} and $^{N,O}L^{3-\bullet}$ in **2**.[17] Notably, this value represents a nearly 40-fold enhancement in the magnetic exchange strength in moving from $^{N,O}L^{2-}$ to $^{N,O}L^{3-\bullet}$, stemming from direct overlap of spin-bearing metal- and ligand-based orbitals, and further highlights the utility of radical ligands to increase the strength of magnetic interactions. Finally, the plot of $\chi_M T$ vs T obtained for $\mathbf{1}^{ox}$ shows a nearly identical profile to that of **1**, with a fit to data giving the coupling constant J = −0.67(1) cm^{-1}. The higher value relative to **1** presumably stems from the absence of a bound DMSO molecule in $\mathbf{1}^{ox}$,

DOI: 10.1021/jacs.6b02485
J. Am. Chem. Soc. 2016, 138, 6583–6590

leading to a Mn coordination number of 6 and consequently stronger interactions of the donor atoms with Mn.

SUMMARY AND OUTLOOK

The foregoing results demonstrate that incorporation of a benzoquinoid ligand into a chain compound can give rise to a material exhibiting solid-state redox switching of optical, magnetic, and electronic properties. The dark green solid $Mn^{II}(^{N,O}L^{2-})$ undergoes a reversible one-electron reduction to afford a dark purple solid that contains $[Mn^{II}(^{N,O}L^{3-\bullet})]^{-}$. Associated with this ligand-centered reduction is a nearly 40-fold enhancement in magnetic exchange coupling strength, from $J = -0.38(1)$ to $-15.6(2)$ cm^{-1}, and a corresponding 10^4-fold enhancement of electronic conductivity, from $\sigma = 2.33(1) \times 10^{-12}$ to $8.61(1) \times 10^{-8}$ S/cm. In addition, the reduction led to a lowering of the thermal activation energy for electron conduction from $E_a = 0.64(1)$ to $0.39(1)$ eV. Work is underway to further investigate the electronic conductivity of these solids, with an emphasis on obtaining single-crystal data, and to incorporate other metal ions into similar structures, with an emphasis on high-anisotropy metals that may give rise to redox-switchable conductive single-chain magnets.

ASSOCIATED CONTENT

Supporting Information

The Supporting Information is available free of charge on the ACS Publications website at DOI: 10.1021/jacs.6b02485.

UV−visible spectra, additional Raman spectra, FT-IR, XAS, conductivity data, XPS (PDF)

Crystallographic information for compound **1** (CIF)

AUTHOR INFORMATION

Corresponding Author

*dharris@northwestern.edu

Notes

The authors declare no competing financial interest.

ACKNOWLEDGMENTS

Work in the Harris lab (I.R.J. and T.D.H.) was supported by the National Science Foundation (NSF) through Grant DMR-1351959, the U.S. Air Force Office of Scientific Research through Grant FA9550-14-1-0274, the Institute for Sustainability and Energy at Northwestern, and Northwestern University (NU). Work in the Dincă lab (L.S. and M.D.) was supported by the U.S. Department of Energy (DOE), Office of Science, Office of Basic Energy Sciences, under Award No. DE-SC0006937. Work in the Van Duyne lab (B.N. and R.P.V.D.) was supported by NSF through Grant CHE-1506683. Purchase of the SQUID magnetometer was supported in part by the International Institute of Nanotechnology (IIN). Beamline 5-BM-D is supported through E. I. duPont de Nemours & Co., NU, The Dow Chemical Co., the State of Illinois through the Department of Commerce and the Board of Education (HECA), the DOE Office of Energy Research, and the NSF Division of Materials Research. The Keck-II Facility of the NU*ANCE* Center and the J. B. Cohen X-ray Diffraction Facility at NU have received support from the NU-MRSEC (NSF DMR-1121262) and IIN, and The Keck-II Facility of the NU*ANCE* Center was also supported by the Soft and Hybrid Nanotechnology Experimental (SHyNE) Resource (NSF NNCI-1542205). We thank Profs. J. T. Hupp and O. K. Farha for use of their dc power supply, Dr. I. Hod for assistance with electrophoretic deposition, Dr. A. Filatov for collecting some of the XPS data, and Dr. Q. Ma for assistance with Beamline 5-BM-D.

REFERENCES

(1) (a) Ortega, N.; Kumar, A.; Scott, J. F.; Katiyar, R. S. *J. Phys.: Condens. Matter* **2015**, *27*, 504002−5040024. (b) Elovaara, T.; Majumdar, S.; Huhtinen, H.; Paturi, P. *Adv. Funct. Mater.* **2015**, *25*, 5030−5037.

(2) (a) Castellano, M.; Ruiz-García, R.; Cano, J.; Ferrando-Soria, J.; Pardo, E.; Fortea-Pérez, F. R.; Stiriba, S.-E.; Julve, M.; Lloret, F. *Acc. Chem. Res.* **2015**, *48*, 510−520. (b) Mas-Torrent, M.; Rovira, C.; Veciana, J. *Adv. Mater.* **2013**, *25*, 462−468.

(3) (a) Di, C.; Zhang, F.; Zhu, D. *Adv. Mater.* **2013**, *25*, 313−330. (b) Orgiu, E.; Samori, P. *Adv. Mater.* **2014**, *26*, 1827−1845.

(4) (a) Jiang, J.; Li, Y.; Liu, J.; Huang, X.; Yuan, C.; Lou, X. W. *Adv. Mater.* **2012**, *24*, 5166−5180. (b) Jost, K. A.; Stenger, D.; Perez, C. R.; McDonough, J.; Lian, K.; Gogotsi, Y.; Dion, G. *Energy Environ. Sci.* **2013**, *6*, 2698−2705.

(5) Manruqie-Juárez, M. D.; Rat, S.; Salmon, L.; Molnár, G.; Quintero, C. M.; Nicu, L.; Shepherd, H. J.; Bousseksou, A. *Coord. Chem. Rev.* **2016**, *308*, 395−408.

(6) (a) Sauthoff, G. *Intermetallics*; Wiley-VCH: Weinheim, Germany, 1995. (b) Chan, J. Y.; Kauzlarich, S. M.; et al. *Chem. Mater.* **1997**, *9*, 3132−3135. (c) Ohno, H. *Science* **1998**, *281*, 951−956. (d) Sato, O.; Iyoda, T.; Fujishima, A.; Hashimoto, K. *Science* **1996**, *272*, 704−705. (e) Saxena, S. S.; Agarwal, P.; Ahilan, K.; Grosche, F. M.; Haselwimmer, R. K. W.; Steiner, M. J.; Pugh, E.; Walker, I. R.; Julian, S. R.; Monthoux, P.; Lonzarich, G. G.; Huxley, A.; Sheikin, I.; Braithwaite, D.; Flouquet, J. *Nature* **2000**, *406*, 587−592. (f) Kittilstved, K. R.; Liu, W. K.; Gamelin, D. R. *Nat. Mater.* **2006**, *5*, 291−297. (g) Eerenstein, W.; Mathur, N. D.; Scott, J. F. *Nature* **2006**, *442*, 759−765. (h) Keizer, R. S.; Goennenwein, S. T. B.; Klapwijk, T. M.; Miao, G.; Xiao, G.; Gupta, A. *Nature* **2006**, *439*, 825−827. (h1) Aguilà, D.; Prado, Y.; Koumousi, E. S.; Mathonière, C.; Clérac, R. *Chem. Soc. Rev.* **2016**, *45*, 203−224.

(7) (a) Coronado, E.; Galán-Mascarós, J. R.; Gómez-García, C.; Laukhin, V. *Nature* **2000**, *408*, 447−449. (b) Coronado, E.; Day, P. *Chem. Rev.* **2004**, *104*, 5419−5448. (c) Hiraga, H.; Miyasaka, H.; Nakata, K.; Kajiwara, T.; Takaishi, S.; Oshima, Y.; Nojiri, H.; Yamashita, M. *Inorg. Chem.* **2007**, *46*, 9661−9671. (d) Galán-Mascarós, J. R.; Coronado, E.; Goddard, P. A.; Singleton, J.; Coldea, A. I.; Wallis, J. D.; Coles, S. J.; Alberola, A. *J. Am. Chem. Soc.* **2010**, *132*, 9271−9273.

(8) Coronado, E.; Martí-Gastaldo, C.; Navarro-Moratalla, E.; Burzurí, E.; Camón, A.; Luis, F. *Adv. Mater.* **2011**, *23*, 5021−5026.

(9) (a) Gómez-Aguirre, L. C.; Pato-Doldán, B.; Mira, J.; Castro-García, S.; Señarís-Rodríguez, M. A.; Sánchez-Andújar, M.; Singleton, J.; Zapf, V. S. *J. Am. Chem. Soc.* **2016**, *138*, 1122−1125. (b) Tian, Y.; Shen, S.; Cong, J.; Yan, L.; Wang, S.; Sun, Y. *J. Am. Chem. Soc.* **2016**, *138*, 782−785.

(10) (a) Bénard, S.; Yu, P.; Coradin, T.; Rivière, E.; Nakatani, K.; Clément, R. *Adv. Mater.* **1997**, *9*, 981−984. (b) Train, C.; Gruselle, M.; Verdaguer, M. *Chem. Soc. Rev.* **2011**, *40*, 3297−3312.

(11) (a) Miyasaka, H.; Motokawa, N.; Chiyo, T.; Takemura, M.; Yamashita, M.; Sagayama, H.; Arima, T.-h. *J. Am. Chem. Soc.* **2011**, *133*, 5338−5345. (b) Mitsumi, M.; Nishitani, T.; Yamasaki, S.; Shimada, N.; Komatsu, Y.; Toriumi, K.; Kitagawa, Y.; Okumura, M.; Miyazaki, Y.; Górska, N.; Inaba, A.; Kanda, A.; Hanasaki, N. *J. Am. Chem. Soc.* **2014**, *136*, 7026−7037.

(12) Schwab, P. F. H.; Diegoli, S.; Biancardo, M.; Bignozzi, C. A. *Inorg. Chem.* **2003**, *42*, 6613−6615. Deibel, N.; Sommer, M.; Hohloch, S.; Schwann, J.; Schweinfurth, D.; Ehret, F.; Sarkar, B. *Organometallics* **2014**, *33*, 4756−4765.

(13) (a) Dei, A.; Gatteschi, D.; Pardi, L.; Russo, U. *Inorg. Chem.* **1991**, *30*, 2589−2594. (b) Min, K. S.; Rheingold, A. L.; DiPasquale, A. G.; Miller, J. S. *Inorg. Chem.* **2006**, *45*, 6135−6137. (c) Min, K. S.; DiPasquale, A. G.; Golen, J. A.; Rheingold, A. L.; Miller, J. S. *J. Am.*

DOI: 10.1021/jacs.6b02485
J. Am. Chem. Soc. 2016, 138, 6583−6590

Chem. Soc. **2007**, *129*, 2360−2368. (d) Guo, D.; McCusker, J. K. *Inorg. Chem.* **2007**, *46*, 3257. (e) Jeon, I.-R.; Park, J. G.; Xiao, D. J.; Harris, T. D. *J. Am. Chem. Soc.* **2013**, *135*, 16845−16848. (f) DeGayner, J. A.; Jeon, I.-R.; Harris, T. D. *Chem. Sci.* **2015**, *6*, 6639−6648.
(14) (a) Heinze, K.; Huttner, G.; Walter, O. *Eur. J. Inorg. Chem.* **1999**, *1999*, 593−600. (b) Gupta, P.; Das, A.; Basuli, F.; Castineiras, A.; Sheldrick, W. S.; Mayer-Figge, H.; Bhattacharya, S. *Inorg. Chem.* **2005**, *44*, 2081−2088. (c) Gaudette, A. I.; Jeon, I.-R.; Anderson, J. S.; Grandjean, F.; Long, G. J.; Harris, T. D. *J. Am. Chem. Soc.* **2015**, *137*, 12617−12626.
(15) Jeon, I.-R.; Negru, B.; Van Duyne, R. P.; Harris, T. D. *J. Am. Chem. Soc.* **2015**, *137*, 15699−15702.
(16) Darago, L. E.; Aubrey, M. L.; Yu, C. J.; Gonzalez, M. I.; Long, J. R. *J. Am. Chem. Soc.* **2015**, *137*, 15703−15711.
(17) Jeon, I.-R.; Harris, T. D. *Chem. Commun.* **2016**, *52*, 1006−1008.
(18) *APEX2*, v. 2009 ; Bruker Analytical X-Ray Systems, Inc: Madison, WI, 2009.
(19) Sheldrick, G. M. *SADABS*, version 2.03, Bruker Analytical X-Ray Systems: Madison, WI, 2000.
(20) Sheldrick, G. M., *SHELXTL*, Version 6.12; Bruker Analytical X-ray Systems, Inc.: Madison, WI, 2000.
(21) Dolomanov, O. V.; Bourhis, L. J.; Gildea, R. J.; Howard, J. A. K.; Puschmann, H. *J. Appl. Crystallogr.* **2009**, *42*, 339−341.
(22) Ravel, B.; Newville, M. *J. Synchrotron Radiat.* **2005**, *12*, 537−541.
(23) Bain, G. A.; Berry, J. F. *J. Chem. Educ.* **2008**, *85*, 532−536.
(24) Wudl, F.; Bryce, M. R. *J. Chem. Educ.* **1990**, *67*, 717−718.
(25) Beckmann, U.; Bill, E.; Weyhermüller, T.; Wieghardt, K. *Inorg. Chem.* **2003**, *42*, 1045−1056.
(26) Hod, I.; Bury, W.; Karlin, D. M.; Deria, P.; Kung, C.; Katz, M. J.; So, M.; Klahr, B.; Jin, D.; Chung, Y.; Odom, T. W.; Farha, O. K.; Hupp, J. T. *Adv. Mater.* **2014**, *26*, 6295−6300.
(27) (a) Wade, C. R.; Li, M.; Dincă, M. *Angew. Chem., Int. Ed.* **2013**, *52*, 13377−13381. (b) Kung, C.-W.; Wang, T. C.; Mondloch, J. E.; Fairen-Jimenez, D.; Gardner, D. M.; Bury, W.; Klingsporn, J. M.; Barnes, J. C.; Van Duyne, R.; Stoddart, J. F.; Wasielewski, M. R.; Farha, O. K.; Hupp, J. T. *Chem. Mater.* **2013**, *25*, 5012−5017.
(28) Abrahams, B. F.; Bond, A. M.; Le, T. H.; McCormick, L. J.; Nafady, A.; Robson, R.; Vo, N. *Chem. Commun.* **2012**, *48*, 11422−11424.
(29) Heo, J.; Jeon, Y.-M.; Mirkin, C. A. *J. Am. Chem. Soc.* **2007**, *129*, 7712−7713.
(30) (a) Hartl, F.; Stufkens, D. J.; Vlček, A. *Inorg. Chem.* **1992**, *31*, 1687−1695. (b) Op't Holt, B. T. O.; Vance, M. A.; Mirica, L. M.; Heppner, D. E.; Stack, T. D. P.; Solomon, E. I. *J. Am. Chem. Soc.* **2009**, *131*, 6421−6438.
(31) Baum, A.; Lindeman, S. V.; Fiedler, A. T. *Chem. Commun.* **2013**, *49*, 6531−6533.
(32) Downes, C. A.; Marinescu, S. C. *J. Am. Chem. Soc.* **2015**, *137*, 13740−13743.
(33) Manceau, A.; Marcus, M. A.; Grangeon, S. *Am. Mineral.* **2012**, *97*, 816−827.
(34) Sun, L.; Hendon, C. H.; Minier, M. A.; Walsh, A.; Dincă. *J. Am. Chem. Soc.* **2015**, *137*, 6164−6167.
(35) Givaja, G.; Amo-Ochoa, P.; Gómez-García, C. J.; Zamora, F. *Chem. Soc. Rev.* **2012**, *41*, 115−147.
(36) (a) Kobayashi, Y.; Jacobs, B.; Allendorf, M. D.; Long, J. R. *Chem. Mater.* **2010**, *22*, 4120−4122. (b) Kambe, T.; Sakamoto, R.; Kusamoto, T.; Pal, T.; Fukui, N.; Hoshiko, K.; Shimojima, T.; Wang, Z.; Hirahara, T.; Ishizaka, K.; Hasegawa, S.; Liu, F.; Nishihara, H. *J. Am. Chem. Soc.* **2014**, *136*, 14357−14360.
(37) Grosso, G.; Parravicini, G. P. *Solid State Physics*; Academic Press: London, 2000.
(38) Fisher, M. E. *Am. J. Phys.* **1964**, *32*, 343−346.
(39) Seiden, J. *J. Phys., Lett.* **1983**, *44*, 947−952.

DOI: 10.1021/jacs.6b02485
J. Am. Chem. Soc. 2016, 138, 6583−6590